Macromolecules

Article

pubs.acs.org/Macromolecules

Side Chain Structure Affects the Photovoltaic Performance of Two-Dimensional Conjugated Polymers

Jian-Ming Jiang, His-Kuei Lin, Yu-Che Lin, Hsiu-Cheng Chen, Shang-Che Lan, Chiao-Kai Chang, and Kung-Hwa Wei*

Department of Materials Science and Engineering, National Chiao Tung University, 300 Hsinchu, Taiwan

Supporting Information

ABSTRACT: We used Stille coupling of electron-rich benzo[1,2-*b*:4,5-*b*′]dithiophene (BDT) presenting conjugated alkylthiophene (T), alkylphenyl (P), or alkylfuran (F) side chains with electron-deficient alkoxy-modified 2,1,3-benzooxadiazole (BO) moieties to obtain a series of two-dimensional, conjugated, D−π−A polymers (PBDTTBO, PBDTPBO, and PBDTFBO). The side chains of the BDT units altered the solubility, conformations, and electronic properties of the synthesized conjugated polymers, allowing tuning of their photovoltaic properties when blended with fullerenes. Density functional theory calculations revealed that the presence of these side chain groups on the BDT donor units affected the torsion angles between the side chain groups and the conjugated main chains but resulted in only slightly different energy levels for the highest occupied molecular orbitals for these polymers, consistent with results obtained experimentally using cyclic voltammetry. These polymers displayed excellent thermal stabilities (5 wt % degradation temperatures: >330 °C) and broad spectral absorptions (from 450 to 700 nm). Transmission electron microscopy images revealed that the morphologies of active layers comprising these two-dimensional conjugated polymers and the fullerene derivative $PC_{71}BM$ did, however, vary substantially depending on the structure of the side chains that affects the solubility of the polymers. As a result, the efficiencies of photovoltaic devices incorporating PBDTFBO, PBDTPBO, or PBDTTBO polymers and $PC_{71}BM$ varied greatly, from 3.6 to 5.9%. When using 1-chloronaphthalene (1 vol %) or 1,8-diiodooctane (1 vol %) as an additive for processing the active layer, the power conversion efficiencies (PCEs) of photovoltaic devices incorporating blends of PBDTFBO, PBDTPBO, or PBDTTBO and $PC_{71}BM$ (1:2) improved to 5.4, 6.4, and 7.4%, respectively, due to their optimized morphologies, with the PCE of 7.4% being among the highest values reported for conjugated polymers involving BO moieties. Thus, the photovoltaic properties of these conjugated polymers were highly tunable through slight modifications of their side chain structures.

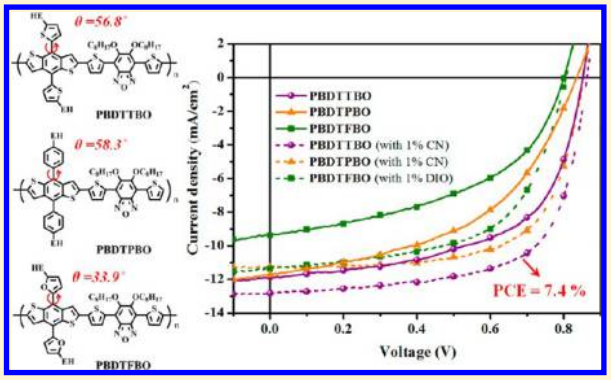

INTRODUCTION

Thin-film polymer solar cells (PSCs) based on bulk heterojunction (BHJ) structures incorporating conjugated polymers possessing delocalized π electrons and fullerene derivatives are being studied extensively because they allow the fabrication of lightweight, large-area, flexible devices using low-cost solution processing methods.[1−3] Tremendous efforts have been made toward improving the power conversion efficiencies (PCEs) of polymer BHJ devices that incorporate conjugated polymers and fullerene derivatives as their electron-donating and -accepting components, respectively.[4−7]

In attempts to harvest more photons and to tune the energy levels, several conjugated polymers have been developed featuring conjugated electron donor/acceptor (D/A) units in main chain[8−19] or two-dimensional conjugated[20−22] configurations. The efficiencies of PSCs can now reach greater than 10% as a result of our better understanding of the photon-to-electron conversion mechanism and the development of novel materials and tandem device architectures.[23−26]

For conjugated polymer materials that are designed to mix with fullerene derivatives to exhibit excellent photovoltaic properties, they must possess (i) suitable band gaps to broaden their absorption range, (ii) crystalline properties to ensure good charge mobility, and (iii) low-lying energy levels for their highest occupied molecular orbital (HOMO) to provide high open-circuit voltages (V_{oc}). Through suitable selection of a weak electron donor (D) and a strong electron acceptor (A), however, it is possible to optimize the energy levels of the HOMO and the band gap of a synthesized D/A polymer simultaneously.

Benzothiadiazole (BT) is one of the stronger electron-withdrawing moieties used widely in PSCs due to a combination of its electron accepting properties and its ability to adopt a quinoid structure, resulting in medium-band-gap, coplanar polymers.[27] Benzooxadiazole (BO) is an electron-

Received: September 14, 2013
Revised: December 7, 2013
Published: December 12, 2013

dx.doi.org/10.1021/ma401897b | Macromolecules 2014, 47, 70−78

deficient heterocycle having a structure similar to that of BT, but with a lower-lying oxidation potential,[28−31] thereby potentially increasing the V_{oc} of corresponding devices containing its blends with fullerene derivatives. Several reports describe the photovoltaic properties of 4,7-dithiophene-substituted BO-based conjugated polymers, with the highest power conversion efficiency having been 5−7%.[32−35]

On the other hand, benzo[1,2-*b*:4,5-*b*′]dithiophene (BDT), a weak electron donor,[36] is attractive for use as an electron-donating unit because of its structural symmetry and rigid fused aromatic system, features that can enhance electron delocalization and improve charge mobility.[37] For instance, thiophene-substituted BDT, 5-alkylthiophene-2-yl-substituted benzo[1,2-*b*:4,5-*b*′]dithiophene (BDTT), moieties have been used extensively as electron donor units over the past two years. Several copolymers of BDTT and various conjugated species, including benzothiadiazole (BT),[38,39] diketopyrrolopyrrole (DPP),[40,41] and thieno[3,4- *b*]thiophene (TT),[42] have exhibited improved thermal stabilities, lower HOMO and LUMO energy levels, higher hole mobilities, and greatly improved photovoltaic performance in comparison with those of their corresponding alkoxy-substituted BDT.[43] To investigate the effect of the side chain substituent, in this study we synthesized three two-dimensional (2D) conjugated D−π−A copolymers having their side chain groups positioned perpendicular to their main chains. Using BDT derivatives modified with alkylthiophene (T), alkylphenyl (P), and alkylfuran (F) conjugated side chains as the donor units, alkoxy-BO as the acceptor unit, and thiophene as the π-bridge, we investigated the effects of the side chains of the BDT donor units on the photovoltaic properties of the resulting conjugated polymers.

EXPERIMENTAL SECTION

Materials and Synthesis. 4,7-Bis(5-bromothien-2-yl)-5,6-bis(octyloxy)benzo[*c*][1,2,5]oxadiazole (**M1**),[29] {4,8-bis[5-(2-ethylhexyl)thien-2-yl]benzo[1,2-*b*:4,5-*b*′]dithiophene-2,6-diyl}bis(trimethylstannane) (**M2**),[32] {4,8-bis[4-(2-ethylhexyl)phenyl]benzo[1,2-*b*:4,5-*b*′]dithiophene-2,6-diyl}bis(trimethylstannane) (**M3**),[40] and {4,8-bis[5-(2-ethylhexyl)furan-2-yl]benzo[1,2-*b*:4,5-*b*′]dithiophene-2,6-diyl}bis(trimethylstannane) (**M4**)[39] were prepared according to reported procedures. [6,6]-Phenyl-C_{61}-butyric acid methyl ester ($PC_{61}BM$) and [6,6]-phenyl-C_{71}-butyric acid methyl ester ($PC_{71}BM$) was purchased from Nano-C. All other reagents were used as received without further purification, unless stated otherwise.

General Procedure for Stille Polymerization: Alternating Polymer PBDTTBO. **M1** (100 mg, 0.143 mmol), **M2** (130 mg, 0.143 mmol), and tri-*o*-tolylphosphine (3.5 mg, 8.0 mol %) were dissolved in dry chlorobenzene (CB, 4 mL) and degassed for 15 min. Pd_2dba_3 (2.6 mg, 2.0 mol %) was added under N_2, and then the reaction mixture was heated at 130 °C for 48 h. After cooling to room temperature, the solution was added dropwise into MeOH (100 mL). The crude polymer was collected, dissolved in $CHCl_3$, and reprecipitated from MeOH. The solid was washed with MeOH, acetone, and $CHCl_3$ in a Soxhlet apparatus. The $CHCl_3$ solution was concentrated and then added dropwise into MeOH. The precipitate was collected and dried under vacuum to give PBDTTBO (98 mg, 62%). ^{1}H NMR (300 MHz, $CDCl_3$): δ 7.71−7.28 (br, 4H), 7.15−6.74 (br, 6H), 4.41−3.90 (br, 4H), 3.35−2.68 (br, 6H), 2.21−0.61 (br, 58H). Anal. Calcd: C, 69.19; H, 7.39; N, 2.44. Found: C, 69.23; H, 7.10; N, 2.54.

Alternating Polymer PBDTPBO. Using a polymerization procedure similar to that described above for PBDTTBO, a mixture of **M1** (100 mg, 0.143 mmol) and **M3** (128 mg, 0.143 mmol) in dry CB (4 mL) was polymerized to give PBDTPBO (109 mg, 69%). ^{1}H NMR (300 MHz, $CDCl_3$): δ 7.73−7.27 (br, 4H), 7.19−6.69 (br, 10H), 4.42−3.91 (br, 4H), 3.37−2.67 (br, 6H), 2.22−0.61 (br, 58H). Anal. Calcd: C, 74.16; H, 7.82; N, 2.47. Found: C, 74.25; H, 7.91; N, 2.52.

Alternating Polymer PBDTFBO. Using a polymerization procedure similar to that described above for PBDTTBO, a mixture of **M1** (100 mg, 0.143 mmol) and **M4** (125 mg, 0.143 mmol) in dry CB (4 mL) was polymerized to give PBDTFBO (102 mg, 66%). ^{1}H NMR (300 MHz, $CDCl_3$): δ 7.70−7.26 (br, 4H), 7.17−6.70 (br, 6H), 4.40−3.91 (br, 4H), 3.36−2.67 (br, 6H), 2.20−0.61 (br, 58H). Anal. Calcd: C, 71.18; H, 7.60; N, 2.52. Found: C, 71.25; H, 7.51; N, 2.48.

Measurements and Characterization. ^{1}H NMR spectra were recorded using a Varian UNITY 300-MHz spectrometer. Thermogravimetric analysis (TGA) was performed using a TA Instruments Q500 apparatus; the thermal stabilities of the samples were determined under a N_2 atmosphere by measuring their weight losses while heating at a rate of 20 °C min^{-1}. Size exclusion chromatography (SEC) was performed using a Waters chromatography unit interfaced with a Waters 1515 differential refractometer; polystyrene was the standard; the temperature of the system was set at 45 °C; $CHCl_3$ was the eluent. UV−vis spectra of dilute solutions (1×10^{-5} M) of samples in dichlorobenzene (DCB) were recorded at room temperature (ca. 25 °C) using a Hitachi U-4100 spectrophotometer. Solid films for UV−vis spectroscopic analysis were obtained by spin-coating the polymer solutions onto a quartz substrate. Cyclic voltammetry (CV) of the polymer films was performed using a BAS 100 electrochemical analyzer operated at a scan rate of 50 mV s^{-1}; the solvent was anhydrous MeCN, containing 0.1 M tetrabutylammonium hexafluorophosphate ($TBAPF_6$) as the supporting electrolyte. The potentials were measured against a Ag/Ag^+ (0.01 M $AgNO_3$) reference electrode; the ferrocene/ferrocenium ion (Fc/Fc^+) pair was used as the internal standard (0.09 V). The onset potentials were determined from the intersection of two tangents drawn at the rising and background currents of the cyclic voltammograms. HOMO and LUMO energy levels were estimated relative to the energy level of the ferrocene reference (4.8 eV below vacuum level). X-ray diffraction (XRD) patterns of the pristine polymer thin films were measured using a Bruker D8 high-resolution X-ray diffractometer operated in grazing incidence mode. Topographic and phase images of the polymer:$PC_{71}BM$ films (surface area: 5×5 μm^2) were obtained using a Digital Nanoscope III atomic force microscope operated in the tapping mode under ambient conditions. The thickness of the active layer of the device was measured using a Veeco Dektak 150 surface profiler. Transmission electron microscopy (TEM) images of the polymer:$PC_{71}BM$ films were recorded using a FEI T12 transmission electron microscope operated at 120 keV.

Fabrication and Characterization of Photovoltaic Devices. Indium tin oxide (ITO)-coated glass substrates were cleaned stepwise in detergent, water, acetone, and isopropyl alcohol (ultrasonication; 20 min each) and then dried in an oven for 1 h; subsequently, the substrates were treated with UV ozone for 30 min prior to use. A thin layer (ca. 20 nm) of poly(ethylenedioxythiophene):polystyrenesulfonate (PEDOT:PSS, Baytron P VP AI 4083) was spin-coated (5000 rpm) onto the ITO substrates. After baking at 140 °C for 20 min in air, the substrates were transferred to a N_2-filled glovebox. The polymer and PCBM were codissolved in DCB at various weight ratios, but at a fixed total concentration, 3 wt % (30 mg mL^{-1}). The blend solutions were stirred continuously for 12 h at 80 °C and then filtered through a PTFE filter (0.2 μm); the photoactive layers were obtained by spin-coating (600−2000 rpm, 60 s) the blend solutions onto the ITO/PEDOT:PSS surfaces. The thickness of each photoactive layer was approximately 90−120 nm. The devices were ready for measurement after thermal deposition (pressure: ca. 1×10^{-6} mbar) of a 20 nm thick film of Ca and then a 100 nm thick Al film as the cathode. The effective layer area of one cell was 0.04 cm^2. The current density−voltage (J−V) characteristics were measured using a Keithley 2400 source meter. The photocurrent was measured under simulated AM 1.5 G illumination at 100 mW cm^{-2} using a Xe lamp-based Newport 66902 150 W solar simulator. A calibrated Si photodiode with a KG-5 filter was employed to confirm the illumination intensity. External quantum efficiencies (EQEs) were measured using an SRF50 system (Optosolar, Germany). A calibrated monosilicon diode

dx.doi.org/10.1021/ma401897b | *Macromolecules* 2014, 47, 70−78

Scheme 1. Synthesis of the Copolymers PBDTTBO, PBDTPBO, and PBDTFBO

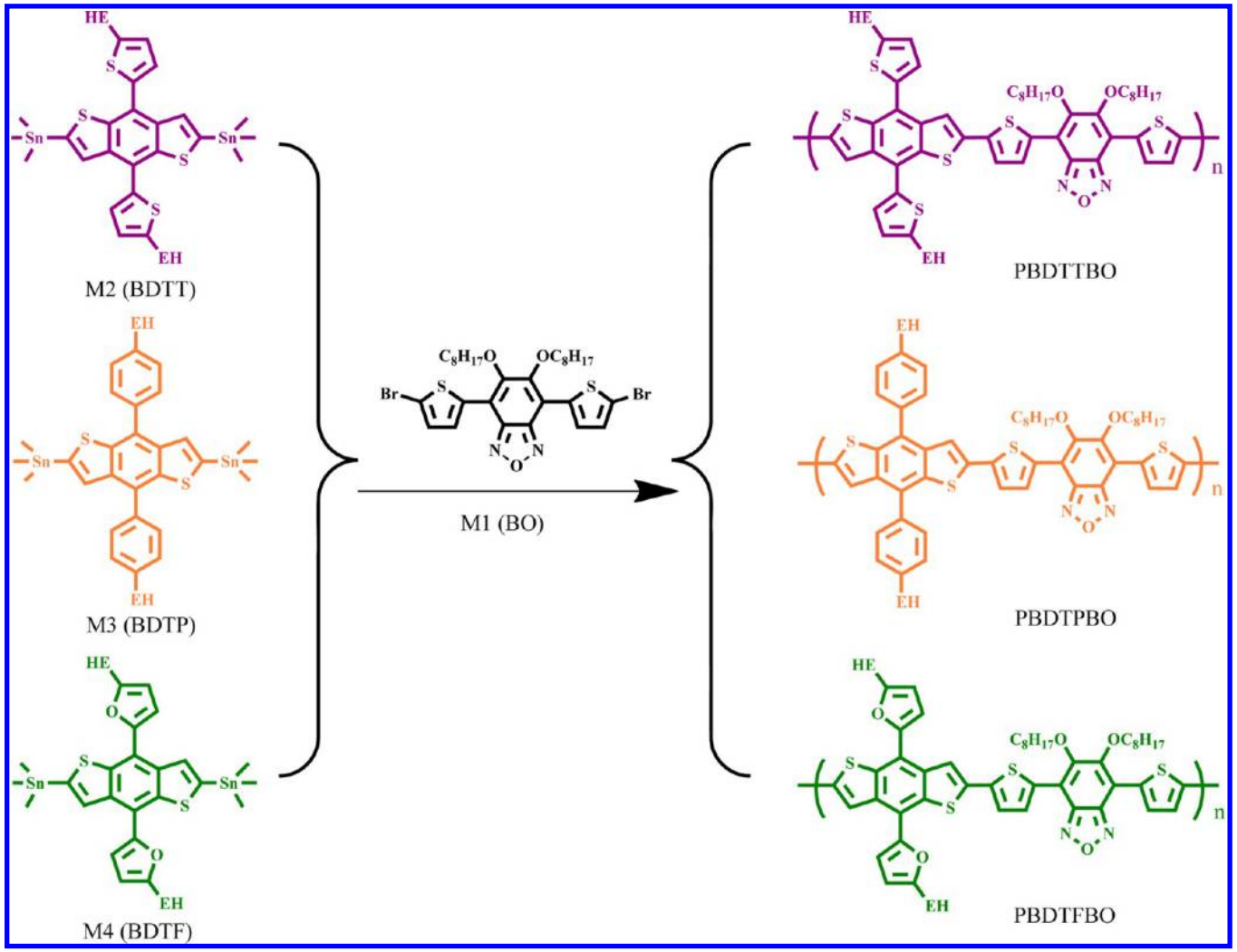

exhibiting a response at 300−800 nm was used as a reference. For hole mobility measurements, hole-only devices were fabricated having the structure ITO/PEDOT:PSS/polymer/Au. The hole mobility was determined by fitting the dark $J-V$ curve into the space-charge-limited current (SCLC) model,[20,44] based on the equation

$$J = \frac{9}{8}\varepsilon_0\varepsilon_r\mu_h\frac{V^2}{L^3}$$

where ε_0 is the permittivity of free space, ε_r is the dielectric constant of the polymer (assumed to be 3.0 for the conjugated polymers), μ_h is the hole mobility, V is the voltage drop across the device, and L is the thickness of the active layer.

RESULTS AND DISCUSSION

Synthesis and Characterization of Synthesized Polymers. Scheme 1 outlines our syntheses of the designed polymers. To ensure good solubility of the BO derivative **M1**, we positioned two neighboring octyloxy chains on the BO ring as reported in previous studies.[29−31] We synthesized **M2**,[32] **M3**,[40] and **M4**[39] using methods reported in the literature. From Stille couplings of **M2**, **M3**, and **M4** with **M1** in the presence of Pd_2dba_3 as the catalyst in CB at 130 °C for 48 h, we obtained the polymers PBDTTBO, PBDTPBO, and PBDTFBO, respectively, in yields of 60−70%. Table 1 lists the number-average (M_n) and weight-average (M_w) molecular weights of these polymers, as determined through size exclusion chromatography (SEC), against polystyrene standards, in $CHCl_3$ as the eluent. Moreover, the solubility of PBDTTBO, PBDTPBO, and PBDTFBO in DCB is determined quantitatively at 25 °C based on the specifications of ASTM E1148;[45] as listed in Table 1, the solubility of PBDTTBO, PBDTPBO, and PBDTFBO is 4.7, 3.5, and 2.1 mg/mL, respectively, at 25 °C.

Table 1. Molecular Weights, Thermal Properties, and Solubility of the Polymers

polymer	M_n[a]	M_w[a]	PDI[a]	T_d[b]	solubility[c] (mg)
PBDTTBO	62.5K	268.8K	4.3	334	4.7
PBDTPBO	64.8K	285.1K	4.4	334	3.5
PBDTFBO	60.6K	284.8K	4.7	334	2.1

[a]Values of M_n, M_w, and PDI of the polymers were determined through GPC (in $CHCl_3$, using polystyrene standards). [b]The 5% weight-loss temperatures (°C) in air. [c]The solubility limit in 1,2-dichlorobenzene (DCB) at 25 °C determined following ASTM E1148.

Thermal Stability. Figure 1 reveals the TGA curves of PBDTTBO, PBDTPBO, and PBDTFBO; their 5% weight-loss temperatures (T_d) were all above 330 °C, indicating good thermal stability—an important characteristic for device fabrication and application.

dx.doi.org/10.1021/ma401897b | *Macromolecules* 2014, 47, 70−78

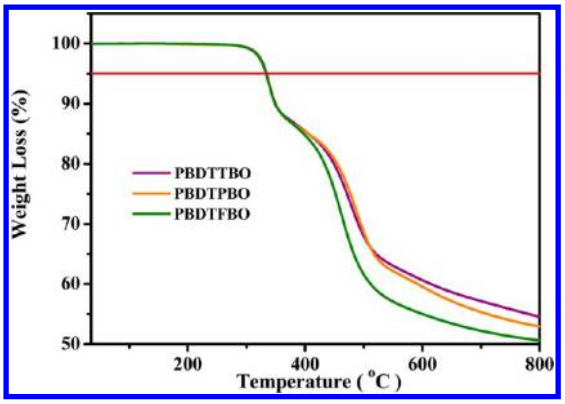

Figure 1. TGA thermograms of the copolymers PBDTTBO, PBDTPBO, and PBDTFBO, recorded at a heating rate of 20 °C min^{-1} under a N_2 atmosphere.

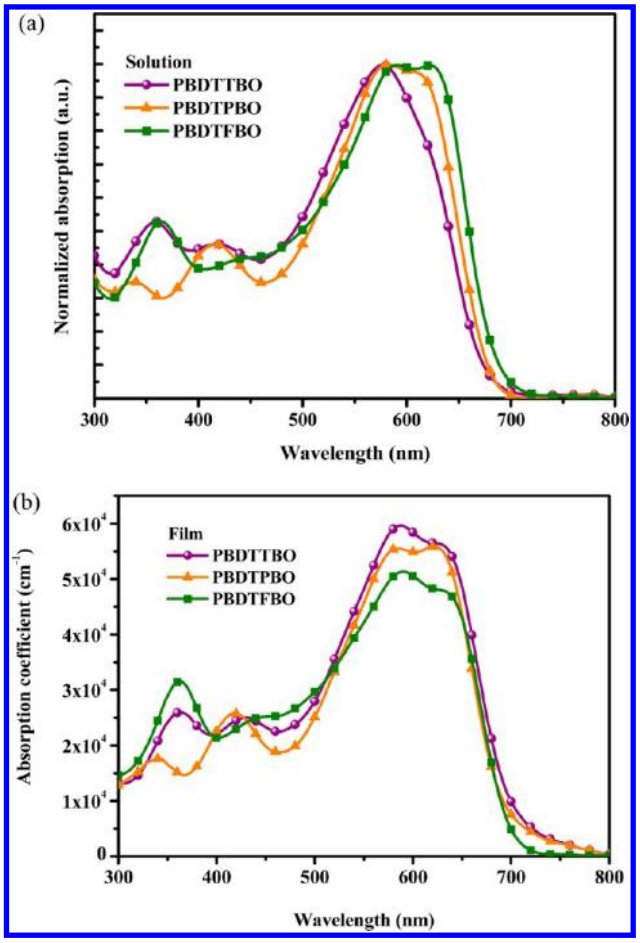

Figure 2. UV−vis absorption spectra of the polymers PBDTTBO, PBDTPBO, and PBDTFBO as (a) dilute solutions (1×10^{-5} M) in DCB and (b) solid films.

Table 2. Optical Properties of the Polymers

	$\lambda_{max,abs}$ (nm)		λ_{onset} (nm)	
	solution	film	film	E_g^{opt} (eV)
PBDTTBO	576	588, 626	697	1.78
PBDTPBO	582, 608	584, 622	690	1.78
PBDTFBO	590, 622	590, 626	697	1.78

Optical Properties. We recorded normalized optical UV−vis absorption spectra of the diluted polymers solutions (in DCB) at room temperature and of their films spin-coated onto quartz substrates. Figure 2a displays the absorption spectra of the solutions of PBDTTBO, PBDTPBO, and PBDTFBO in DCB at room temperature; each absorption spectrum, recorded from a dilute DCB solution, featured two absorption bands: one at 350−450 nm, which we assign to localized $\pi-\pi^*$ transitions, and another, broad band from 500 to 650 nm (i.e., in the long wavelength region), corresponding to intramolecular charge transfer (ICT) between the acceptor (BO) and donor (BDT) units. The absorption spectra of the three polymers in the solid state were similar to their corresponding solution spectra, with slight red-shifts (ca. 5−20 nm) of their absorption maxima, indicating that some intermolecular interactions existed in the solid state. Table 2 summarizes the optical data, including the absorption peak wavelengths ($\lambda_{max,abs}$), absorption edge wavelengths ($\lambda_{edge,abs}$), and optical band gaps (E_g^{opt}) of PBDTTBO, PBDTPBO, and PBDTFBO; in each case, the E_g^{opt} was equal to 1.78 eV.

Electrochemical Properties. We used CV to measure the electrochemical behavior of PBDTTBO, PBDTPBO, and PBDTFBO and, thereby, determine their HOMO and LUMO energy levels. Figure S1 (Supporting Information) displays the electrochemical properties of the solid polymers films; Table 3 summarizes the data. Partially irreversible p-doping/dedoping (oxidation/rereduction) processes occurred for these polymers in the positive potential range—except for PBDTPBO, which underwent a reversible oxidation. In addition, reversible n-doping/dedoping (reduction/reoxidation) processes occurred in the negative potential range for each of these polymers. The onset oxidation potentials (E_{onset}^{ox}, vs Ag/Ag^+) for PBDTTBO, PBDTPBO, and PBDTFBO were 0.66, 0.60, and 0.58 V, respectively; their onset reduction potentials (E_{onset}^{red}) were −1.33, −1.34, and −1.36 V, respectively. On the basis of these onset potentials, we estimated the HOMO and LUMO energy levels, according to the energy level of the ferrocene reference (4.8 eV below vacuum level).[46−48] The HOMO energy levels of PBDTTBO, PBDTPBO, and PBDTFBO were −5.46, −5.40, and −5.38 eV, respectively; the slight variations indicate minor modulations of the ICT strength induced by the electronic effects of the side chains of the BDT moieties. Figure 3 reveals that the LUMO energy levels of PBDTTBO, PBDTPBO, and PBDTFBO were located within the range from −3.44 to −3.47 eV—that is, they were significantly higher than that (ca. −4.0 eV) of $PC_{71}BM$; thus, we expected efficient charge transfer/dissociation to occur in their corresponding devices.[49−51] Moreover, the HOMO energy level of PBDTTBO was 0.05 eV lower than those of PBDTPBO and PBDTFBO, implying that the alkylthienyl side group was slightly more effective at lowering the HOMO energy level in these 2D conjugated polymer structures. In addition, the electrochemical band gaps (E_g^{ec}) of PBDTTBO, PBDTPBO, and PBDTFBO, estimated from the differences between the onset potentials for oxidation and reduction, were very similar, in the range 1.94−1.99 eV. The discrepancies between the electrochemical and optical band gaps presumably resulted from the exciton binding energies of the polymers and/or the interfacial barriers for charge injection.[52]

Computational Study. We employed density functional theory (B3LYP/6-31G** level) to perform quantum chemistry calculations of the electronic structures of these polymers. To simplify the calculations, we replaced the long alkyl side chains

dx.doi.org/10.1021/ma401897b | *Macromolecules* 2014, 47, 70−78

Table 3. Electrochemical Properties of the Polymers PBDTTBO, PBDTPBO, and PBDTFBO

	E_{onset}^{ox} (V)	E_{onset}^{red} (V)	HOMO[a] (eV)	LUMO[a] (eV)	E_g^{ec} (eV)	HOMO[b] (eV)	LUMO[b] (eV)
PBDTTBO	0.66	−1.33	−5.46	−3.47	1.99	−4.90	−2.52
PBDTPBO	0.60	−1.34	−5.40	−3.46	1.94	−4.88	−2.50
PBDTFBO	0.58	−1.36	−5.38	−3.44	1.94	−4.78	−2.52

[a]HOMO and LUMO energy levels estimated from the oxidation and reduction peaks, respectively, of the cyclic voltammograms. [b]HOMO and LUMO energy levels calculated using density functional theory (DFT).

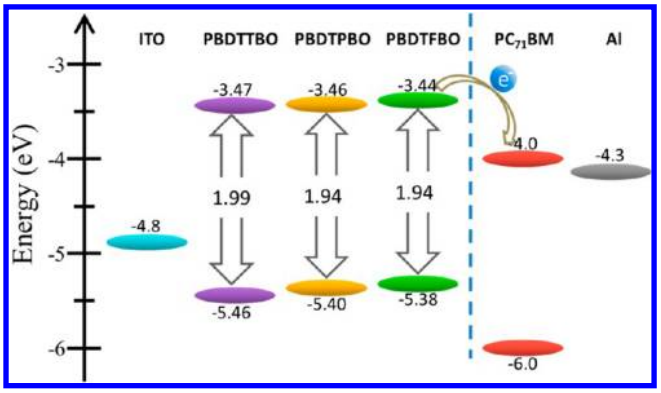

Figure 3. Energy level diagram for PBDTTBO, PBDTPBO, and PBDTFBO.

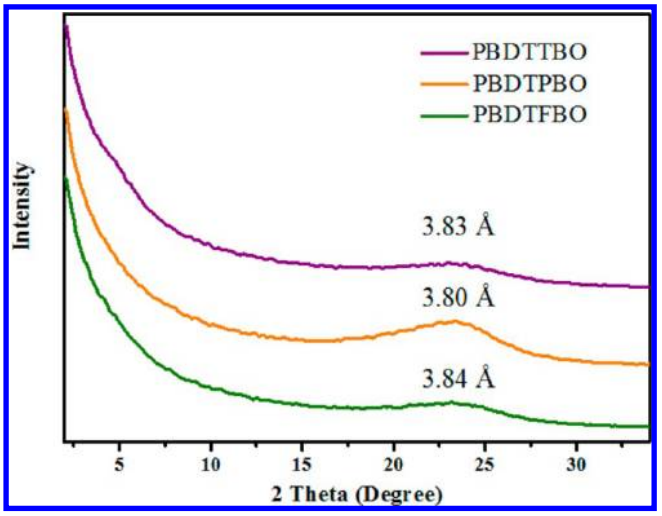

Figure 4. XRD patterns of pristine PBDTTBO, PBDTPBO, and PBDTFBO.

by methyl groups. Table 3 lists the calculated HOMO and LUMO energy levels; Table 4 displays the simulated electron density distributions and the torsion angles between the main chains of the conjugated polymers and the side chain groups. The calculated HOMOs featured extended delocalization along the entire conjugated backbone, affected by both the donor and acceptor units, as did the calculated densities of states for the LUMOs, but with more of an effect on the acceptor units. Moreover, the wave functions of the HOMOs of PBDTTBO, PBDTPBO, and PBDTFBO can be delocalized onto the aromatic rings, indicating that the π electrons were delocalized better within the 2-D conjugated structures. Because a furan ring has lower steric bulk than a thiophene or benzene ring, the torsion angle between the alkylfuranyl group and the backbone unit in PBDTFBO was lower than those in PBDTTBO and PBDTPBO. Thus, the lower torsion angles between the alkylfuranyl groups and the backbone unit in PBDTFBO allowed more effective electron conjugated length over the electron-donating alkylfuranyl side chain, thereby providing a HOMO energy level that was higher than those of the other two polymers.[53] The different absorption coefficients of the three polymers were attributed to the various torsion angles between the side chain group and the backbone that cause the diverse oscillator strength and influence the absorption energy.[54]

XRD Patterns. The grazing-incidence XRD patterns of PBDTTBO, PBDTPBO, and PBDTFBO in Figure 4 featured weak reflections at 23.2°, 23.4°, and 23.1°, respectively, due to their (010) planes, corresponding to distances of 3.83, 3.80, and 3.84 Å, respectively, suggesting facial $\pi-\pi$ stacking of the polymeric chains that would favor charge transport in their films.[55]

Hole Mobility. Figure 5 displays the hole mobilities of devices incorporating the polymer/$PC_{71}BM$ blends at a blend ratio of 1:2 (w/w). The hole mobilities that is determined between the voltage drop of 0.8−1.6 V in the PBDTTBO, PBDTPBO, and PBDTFBO blends with $PC_{71}BM$ were 3.7 ×

Table 4. Simulated HOMO and LUMO Electron Density Distributions of PBDTTBO, PBDTPBO, and PBDTFBO, Determined through DFT Calculations

Polymer	Structure	θ (°)	HOMO orbital	LUMO orbital
PBDTTBO	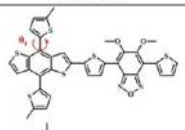	56.8	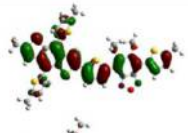	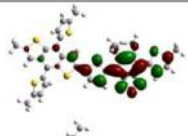
PBDTPBO	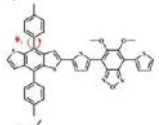	58.3	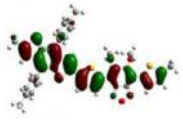	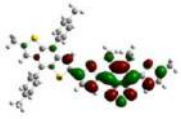
PBDTFBO	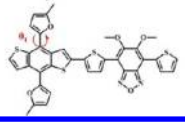	33.9	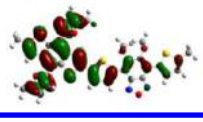	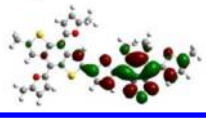

dx.doi.org/10.1021/ma401897b | *Macromolecules* 2014, 47, 70−78

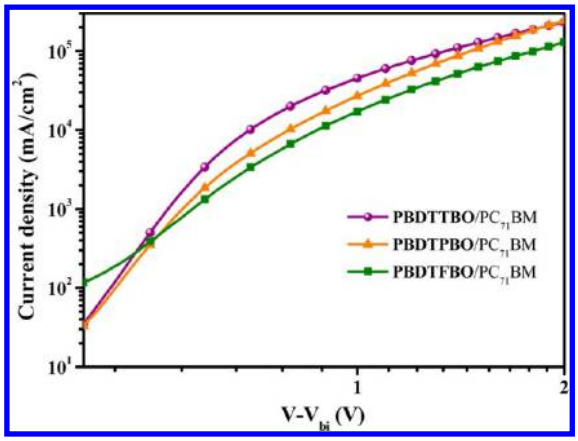

Figure 5. Dark $J-V$ curves of hole-dominated carrier devices incorporating the polymers blended with $PC_{71}BM$ [blend ratio, 1:2 (w/w)].

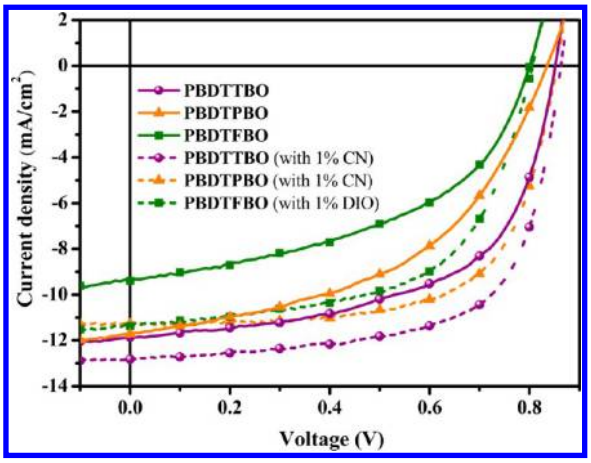

Figure 6. $J-V$ characteristics of PSCs incorporating polymer:$PC_{71}BM$ blends [blend ratio, 1:2 (w/w)].

10^{-2}, 1.8×10^{-2}, and 9.1×10^{-3} cm^2 V^{-1} s^{-1}, respectively; the hole mobility in the PBDTTBO blend is 4 times as large as in the PBDTFBO blends with $PC_{71}BM$.

Photovoltaic Properties and Active Layer Morphology. Next, we investigated the photovoltaic properties of the polymers in BHJ solar cells having the sandwich structure ITO/PEDOT:PSS/polymer:$PC_{71}BM$ (1:2, w/w)/Ca/Al, with the photoactive layers having been spin-coated from DCB solutions of the polymer and $PC_{71}BM$. After testing several compositions, the optimized weight ratio for the polymer and $PC_{71}BM$ was found to be 1:2.

Figure 6 presents the $J-V$ curves of these PSCs; Table 5 summarizes the PCEs. The devices prepared from the blends of PBDTTBO, PBDTPBO, and PBDTFBO with $PC_{71}BM$ exhibited open-circuit voltages (V_{oc}) of 0.85, 0.84, and 0.80 V, respectively, corresponding to the difference between the HOMO energy level of the polymer and the LUMO energy level of $PC_{71}BM$.[56] The short-circuit current densities (J_{sc}) of

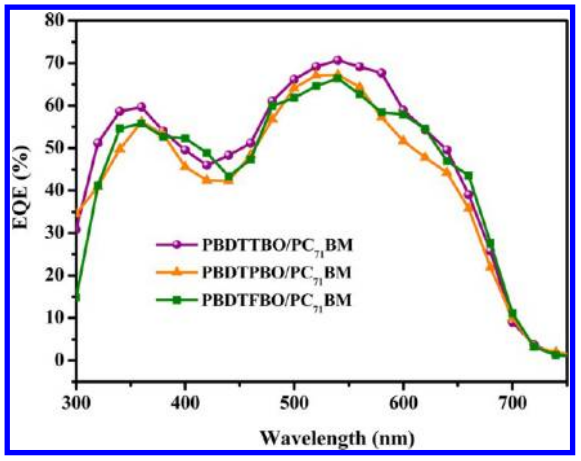

Figure 7. EQE curves of PSCs incorporating polymer:$PC_{71}BM$ blends.

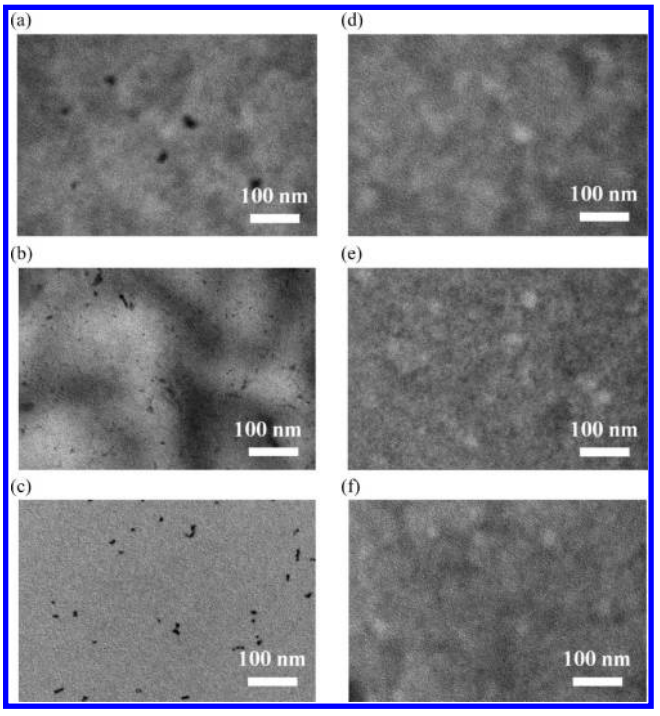

Figure 8. TEM images of polymer:$PC_{71}BM$ (1:2, w/w) blends incorporating (a) PBDTTBO, (b) PBDTPBO, (c) PBDTFBO, (d) PBDTTBO and 1 vol % CN, (e) PBDTPBO and 1 vol % CN, and (f) PBDTFBO and 1 vol % DIO.

Table 5. Photovoltaic Properties of PSCs Incorporating PBDTTBO, PBDTPBO, and PBDTFBO

polymer/$PC_{71}BM$ (1:2)	V_{oc} (V)	J_{sc} (mA cm^{-2})	η (%)	FF (%)	mobility (cm^2 V^{-1} s^{-1})	thickness (nm)
PBDTTBO	0.85	11.8	5.9	59	N/A	90
PBDTPBO	0.84	11.7	4.8	48	N/A	112
PBDTFBO	0.80	9.3	3.6	48	N/A	115
PBDTTBO[a]	0.86	12.8	7.4	67	3.7×10^{-2}	97
PBDTPBO[a]	0.85	11.8	6.4	64	1.8×10^{-2}	117
PBDTFBO[b]	0.81	11.2	5.4	60	9.1×10^{-3}	113

[a]Processed with CN (1 vol %). [b]Processed with DIO (1 vol %).

dx.doi.org/10.1021/ma401897b | *Macromolecules* 2014, 47, 70−78

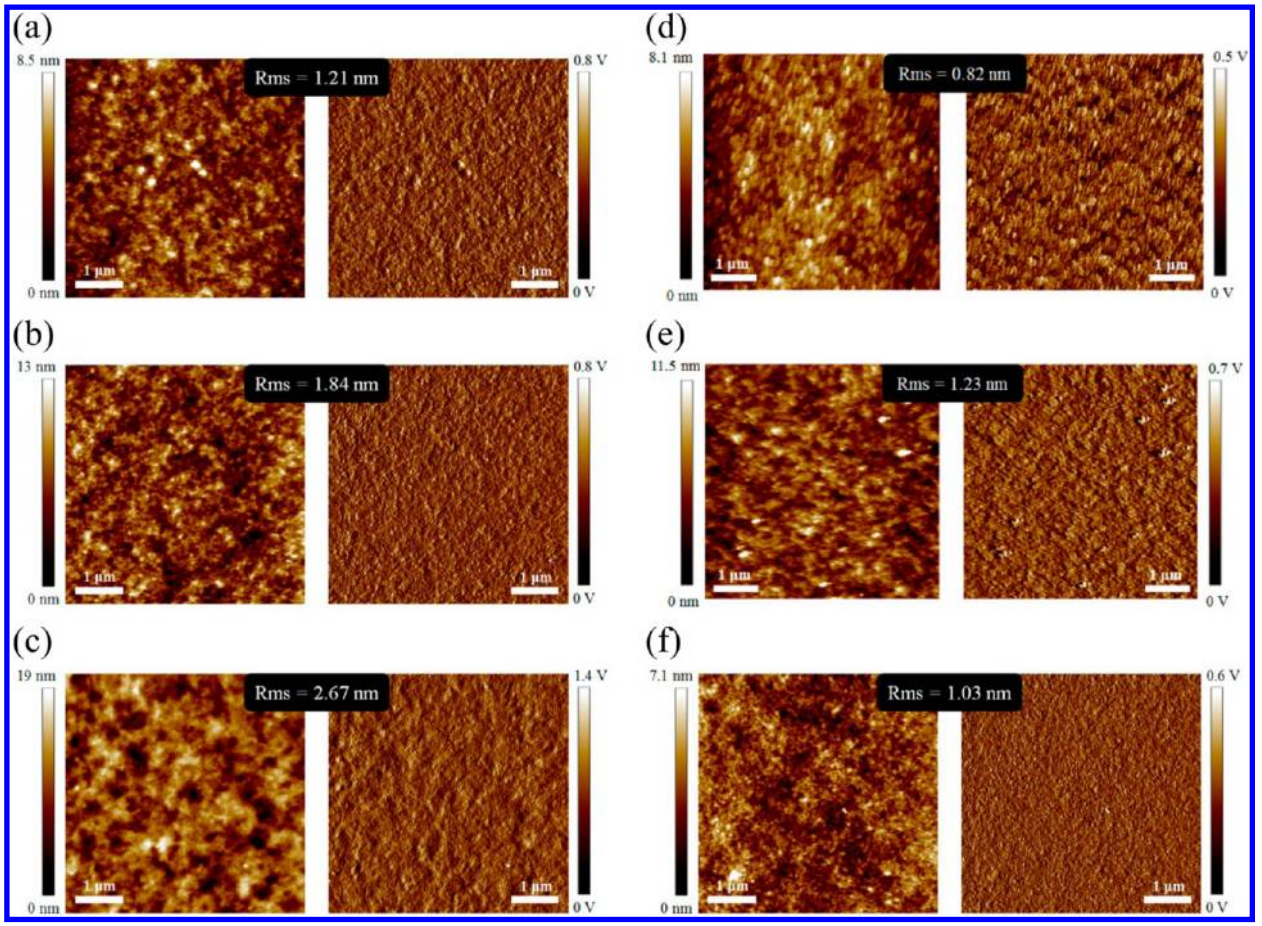

Figure 9. Topographic AFM images of polymer:$PC_{71}BM$ (1:2, w/w) blends incorporating (a) PBDTTBO, (b) PBDTPBO, (c) PBDTFBO, (d) PBDTTBO processed in the presence of CN (1 vol %), (e) PBDTPBO processed in the presence of CN (1 vol %), and (f) PBDTFBO processed in the presence of DIO (1 vol %).

the devices incorporating PBDTTBO, PBDTPBO, and PBDTFBO and $PC_{71}BM$ were 11.8, 11.7, and 9.3 mA cm^{-2}, respectively; The FF of the device incorporating PBDTTBO:$PC_{71}BM$ (1:2, w/w) is 22% higher relatively to that of the device incorporating PBDTPBO or PBDTFBO:$PC_{71}BM$ (1:2, w/w) (0.59 vs 0.48). The differences in the values of J_{sc} and FF for these three cases most likely resulted from the difference in their active layer morphology, which is induced by the large disparity in the polymers' solubility. To improve the morphology of the active layer, we also added a small amount of 1,8-diiodooctane (DIO; 0.5−3 vol %, relative to DCB) or 1-chloronaphthalene (CN; 0.5−3 vol %, relative to DCB) to process these blends. When we added DIO and CN to the solvents for processing the polymer:$PC_{71}BM$ (1:2, w/w) blends, the values of J_{sc} of the devices comprising PBDTTBO, PBDTPBO, and PBDTFBO and $PC_{71}BM$ increased slightly to 12.8, 11.8, and 11.2 mA cm^{-2}, respectively; we suspect that these large variations arose mainly from the different morphologies of the active layers, as evidenced by the much larger hole mobility value of PBDTTBO with $PC_{71}BM$ than that of PBDTFBO with $PC_{71}BM$ in Figure 5. Figure 7 displays the EQE curves of the devices incorporating the polymer:$PC_{71}BM$ blends at weight ratios of 1:2, prepared with 1 vol % CN as the additive for PBDTTBO and PBDTPBO and 1 vol % DIO as the additive for PBDTFBO. The theoretical short-circuit current densities obtained from integrating the EQE curves of the PBDTTBO, PBDTPBO, and PBDTFBO blends were 12.0, 11.4, and 10.8 mA cm^{-2}—values that agree reasonably with the measured (AM 1.5 G) values of J_{sc} of 12.8, 11.8, and 11.2 mA cm^{-2}, respectively, with discrepancies of less than 5%. We attribute the highest value of J_{sc} of PBDTTBO to its superior morphology and a slightly higher absorption coefficient between 550 and 650 nm (Figure 2b and Figure S2). The higher FF of the device incorporating PBDTTBO:$PC_{71}BM$ (1:2, w/w) as the active layer when using 1 vol % CN as the additive was likely due to the fact that the hole mobility in the PBDTTBO:$PC_{71}BM$ (1:2, w/w) blend was larger than those in the PBDTPBO:$PC_{71}BM$ and PBDTFBO:$PC_{71}BM$ blends (Figure 5) and was strongly dependent on the morphology of the film.

Figures 8a−c display TEM images of thin films of PBDTPBO, PBDTPBO, and PBDTFBO blended with $PC_{71}BM$ (1:2, w/w), respectively; the polymer and $PC_{71}BM$ domains appear as bright and the dark regions, respectively, owing to their different degrees of electron scattering. The image in Figure 8a reveals a few ambiguously aggregated $PC_{71}BM$ domains within the moderately homogeneous PBDTTBO/$PC_{71}BM$ blend film; the image in Figure 8b (PBDTPBO/$PC_{71}BM$ blend film) reveals a large phase-separated system with large diffused $PC_{71}BM$ domains dispersed in the polymer matrix with many spots representing undissolved $PC_{71}BM$; the image in Figure 8c reveals vivid $PC_{71}BM$ aggregates in the PBDTFBO/$PC_{71}BM$ blend films. Figures 8d−f display the much more homogeneous morphol-

dx.doi.org/10.1021/ma401897b | *Macromolecules* 2014, 47, 70−78

ogies of the PBDTTBO/$PC_{71}BM$, PBDTPBO/$PC_{71}BM$, and PBDTFBO/$PC_{71}BM$ blend films after we had used additives [i.e., CN (1 vol %) or DIO (1 vol %)] in their processing; thus, the presence of the additives improved the miscibility of the PBDTTBO, PBDTPBO, and PBDTFBO chains with $PC_{71}BM$. The improved morphologies of these active layers enhanced the short-circuit current densities of the devices by 1−20% (from 11.8, 11.7, and 9.3 mA cm^{-2} for the PBDTTBO, PBDTPBO, and PBDTFBO blends prepared without additives, respectively, to 12.8, 11.8, and 11.2 mA cm^{-2} for the blends prepared with additives, respectively). Figure 9 displays atomic force microscopy (AFM) images of films of the blends of the synthesized polymers and $PC_{71}BM$, with the samples having being prepared using procedures identical to those used to fabricate the active layers in the devices. We observed rather smooth surfaces (rms = 1.2−2.6 nm) for the thin films of these polymer blends prepared without the additives (Figures 9a−c). Furthermore, when we incorporated an additive into the processing of these polymer/$PC_{71}BM$ blends, the surface roughnesses decreased (rms = 0.8−1.2 nm; Figures 9d−f). The power conversion efficiencies of the devices incorporating PBDTTBO, PBDTPBO, or PBDTTFBO with $PC_{71}BM$ that were processed involving CN or DIO additive are all improved but with different extent, as compared to that of the devices that were processed without additives. To the best of our knowledge, to date, no literatures on the detailed mechanism of the effect of different kinds of additives on the structural evolution of the blends in the active layer have been reported. We suspect that different additives have different extent of interactions with fullerene and polymers in the molecule level, and hence no coherent mechanism has emerged due to the complicated system. In general, DIO has a boiling point is higher than that of CN and therefore gives more time for the molecules in the active layer to reach equilibrium for the DIO case, but in reality the molecular function of the additives has also to be accounted for. In the near future, we will try to probe the molecular function of the additives.

CONCLUSIONS

We have used Stille coupling polymerization to prepare a series of new conjugated polymers featuring BDT units, presenting conjugated T, P, and F side chains, copolymerized with alkoxy-modified 2,1,3-benzooxadiazole (BO) moieties. These polymers, PBDTTBO, PBDTPBO, and PBDTFBO, exhibited broad absorptions, good thermal stabilities, and suitable energy levels, making them promising materials for solar cell applications. DFT calculations suggested that the nature of the side chain group of the BDT donor units affected the torsion angles between the side chain groups and the conjugated main chains, but resulted in only slightly different electronic properties. The steric bulk of the side chain groups appeared to greatly affect the miscibility of the synthesized polymers with $PC_{71}BM$; the PCEs of photovoltaic devices incorporating these polymers and $PC_{71}BM$ varied greatly, from 3.6 to 5.9%. A device incorporating PBDTTBO and $PC_{71}BM$ (1:2, w/w), with CN (1 vol %) used as an additive for the processing of the active layer, exhibited an excellent morphology and a value of V_{oc} of 0.86 V, a value of J_{sc} of 12.8 mA cm^{-2}, a FF of 0.67, and a PCE of 7.4%; thus, it is possible to tune the photovoltaic properties of these 2D conjugated polymers presenting different conjugated side chains.

ASSOCIATED CONTENT

Supporting Information

Cyclic voltammograms, UV−vis absorption spectra, and $J-V$ characteristics of the three polymers shown in Figures S1−S3 and Table S1. This material is available free of charge via the Internet at http://pubs.acs.org.

AUTHOR INFORMATION

Corresponding Author

*E-mail: khwei@mail.nctu.edu.tw (K.-H.W.).

Notes

The authors declare no competing financial interest.

ACKNOWLEDGMENTS

We thank the National Science Council, Taiwan, for financial support (NSC 102-3113-P-009-002).

REFERENCES

(1) Yu, G.; Gao, J.; Hummelen, J. C.; Wudl, F.; Heeger, A. J. *Science* **1995**, *270*, 1789.
(2) Wienk, M. M.; Koon, J. M.; Verhees, W. J. H.; Knol, J.; Hummelen, J. C.; Van Hal, P. A.; J. Janssen, R. A. *Angew. Chem., Int. Ed.* **2003**, *42*, 3371.
(3) Dennler, G.; Scharber, M. C.; Brabec, C. J. *Adv. Mater.* **2009**, *21*, 1323.
(4) Su, Y. W.; Lan, S. C.; Wei, K. H. *Mater. Today* **2012**, *15*, 554.
(5) Jiang, J. M.; Yuan, M. C.; Dinakaran, K.; Hariharan, A.; Wei, K. H. *J. Mater. Chem. A* **2013**, *1*, 4415.
(6) Vandewal, K.; Himmelberger, S.; Salleo, A. *Macromolecules* **2013**, *46*, 6379.
(7) Kouijzer, S.; Michels, J. J.; Berg, M. V. D.; Gevaerts, V. S.; Turbiez, M.; Wienk, M. M.; Janssen, R. A. J. *J. Am. Chem. Soc.* **2013**, *135*, 12057.
(8) Amb, C. M.; Chen, S.; Graham, K. R.; Subbiah, J.; Small, C. E.; So, F.; Reynolds, J. R. *J. Am. Chem. Soc.* **2011**, *133*, 10062.
(9) Duan, R.; Ye, L.; Guo, X.; Huang, Y.; Wang, P.; Zhang, S.; Zhang, J. P.; Hou, L.; Hou, J. H. *Macromolecules* **2012**, *45*, 3032.
(10) Huang, Y.; Guo, X.; Liu, F.; Huo, L.; Chen, Y.; Russell, T. P.; Han, C. C.; Li, Y.; Hou, J. *Adv. Mater.* **2012**, *24*, 3383.
(11) Qian, D.; Ye, L.; Zhang, M.; Liang, Y.; Li, L.; Huang, Y.; Guo, X.; Zhang, S.; Tan, Z. A.; Hou, J. *Macromolecules* **2012**, *45*, 9611.
(12) Guo, X.; Zhou, N.; Lou, S. J.; Hennek, J. W.; Ortiz, R. P.; Butler, M. R.; Boudreault, P. L. T.; Strzalka, J.; Morin, P. O.; Leclerc, M.; Navarrete, J. T. L.; Ratner, M. A.; Chen, L. X.; Chen, R. P. H.; Facchetti, A.; Marks, T. J. *J. Am. Chem. Soc.* **2012**, *134*, 18427.
(13) Xu, Y. X.; Chuen, C. C.; Yip, H. L.; Ding, F. Z.; Li, Y. X.; Li, C. Z.; Li, X.; Chen, W. C.; Jen, A. K. Y. *Adv. Mater.* **2012**, *24*, 6356.
(14) Meager, I.; Ashraf, R. S.; Rossbauer, S.; Bronstein, H.; Donaghey, J. E.; Marshall, J.; Schroeder, B. C.; Heeney, M.; Anthopoulous, T. D.; McCulloch, I. *Macromolecules* **2013**, *46*, 5961.
(15) Meager, I.; Ashraf, R. S.; Mollinger, S.; Schroeder, B. C.; Bronstein, H.; Beatrup, D.; Vezie, M. S.; Kirchartz, T.; Salleo, A.; Nelson, J.; McCulloch, I. *J. Am. Chem. Soc.* **2013**, *135*, 11537.
(16) Intemann, J. J.; Yao, K.; Yip, H. L.; Xu, Y. X.; Li, Y. X.; Liang, P. W.; Ding, F. Z.; Li, X.; Jen, A. K. Y. *Chem. Mater.* **2013**, *25*, 3188.
(17) Li, Y.; Zou, J.; Yip, H. L.; Li, C. Z.; Zhang, Y.; Chueh, C. C.; Intemann, J.; Xu, Y.; Liang, P. W.; Chen, Y.; Jen, A. K. Y. *Macromolecules* **2013**, *46*, 5497.
(18) Chen, G. Y.; Chen, Y. H.; Chou, Y. J.; Su, M. S.; Chen, C. M.; Wei, K. H. *Chem. Commun.* **2011**, *47*, 5064.
(19) Yuan, M. C.; Chiu, M. Y.; Chain, C. M.; Wei, K. H. *Macromolecules* **2010**, *43*, 6270.
(20) Chang, Y. T.; Hsu, S. L.; Su, M. H.; Wei, K. H. *Adv. Mater.* **2009**, *21*, 2093.
(21) Huang, F.; Chen, K. S.; Yip, H. L.; Hau, S. K.; Acton, O.; Zhang, Y.; Luo, J.; Jen, A. K. Y. *J. Am. Chem. Soc.* **2009**, *131*, 13886.

(22) Kuo, C. Y.; Huang, Y. C.; Hsion, C. Y.; Yang, Y. W.; Huang, C. I.; Rwei, S. P.; Wang, H. L.; Wang, L. *Macromolecules* **2013**, *46*, 5985.
(23) You, J.; Dou, L.; Yoshimura, K.; Kato, T.; Ohya, K.; Moriarty, T.; Emery, K.; Chen, C. C.; Gao, J.; Li, G.; Yang, Y. *Nat. Commun.* **2013**, *4*, 1446.
(24) You, J.; Chen, C. C.; Hong, Z.; Yoshimura, K.; Ohya, K.; Xu, R.; Ye, S.; Gao, J.; Li, G.; Yang, Y. *Adv. Mater.* **2013**, *25*, 3973.
(25) Li, K.; Li, Z.; Feng, K.; Xu, X.; Wang, L.; Peng, Q. *J. Am. Chem. Soc.* **2013**, *135*, 13549.
(26) Li, W.; Furlan, A.; Hendriks, K. H.; Wienk, M. M.; Janssen, R. A. J. *J. Am. Chem. Soc.* **2013**, *135*, 5529.
(27) Peet, J.; Kim, J. Y.; Coates, N. E.; Ma, W. L.; Moses, D.; Heeger, A. J.; Bazan, G. C. *Nat. Mater.* **2007**, *65*, 497.
(28) Blouin, N.; Michaud, A.; Gendron, D.; Wakim, S.; Blair, E.; Plesu, R. N.; Belletete, M.; Durocher, G.; Tao, Y.; Leclerc, M. *J. Am. Chem. Soc.* **2008**, *130*, 732.
(29) Jiang, J. M.; Yang, P. A.; Chen, H. C.; Wei, K. H. *Chem. Commun.* **2011**, *47*, 8877.
(30) Jiang, J. M.; Yang, P. A.; Hsieh, T. H.; Wei, K. H. *Macromolecules* **2011**, *44*, 9155.
(31) Jiang, J. M.; Yang, P. A.; Yu, C. M.; Lin, H. K.; Huang, K. C.; Wei, K. H. *J. Polym. Sci., Part A: Polym. Chem.* **2012**, *50*, 3960.
(32) Liu, B.; Chen, X.; He, Y.; Li, Y.; Xu, X.; Xiao, L.; Li, L.; Zou, Y. *J. Mater. Chem. A* **2013**, *1*, 570.
(33) Wang, Y.; Liu, Y.; Chen, S. J.; Peng, R.; Ge, Z. Y. *Chem. Mater.* **2013**, *25*, 3196.
(34) Jiang, J. M.; Chen, H. C.; Lin, H. K.; Lan, S. C.; Liu, C. M.; Yu, C. M.; Wei, K. H. *Polym. Chem.* **2013**, *4*, 5321.
(35) Kang, T. E.; Cho, H. H.; Kim, H. J.; Lee, W.; Kang, H.; Kim, B. J. *Macromolecules* **2013**, *46*, 6806.
(36) Zhou, H.; Yang, L.; Stoneking, S.; You, W. *ACS Appl. Mater. Interface* **2010**, 1377.
(37) Pan, H.; Li, Y.; Wu, Y.; Liu, P.; Ong, B. S.; Zhu, S.; Xu, G. *J. Am. Chem. Soc.* **2007**, *129*, 4112.
(38) Hou, L. J.; Hou, J. H.; Zhang, S.; Chen, H. Y.; Yang, Y. *Angew. Chem., Int. Ed.* **2010**, *49*, 1500.
(39) Zhang, Y.; Gao, L.; He, C.; Sun, Q.; Li, Y. F. *Polym. Chem.* **2013**, *4*, 1474.
(40) Dou, L.; Gao, J.; Richard, E.; You, J.; Chen, C. C.; Cha, K. C.; He, Y.; Li, G.; Yang, Y. *J. Am. Chem. Soc.* **2012**, *134*, 10071.
(41) Li, W.; Roelofs, W. S. C.; Wienk, M. M.; Janssen, R. A. J. *J. Am. Chem. Soc.* **2012**, *134*, 13787.
(42) Hou, L.; Zhang, S.; Guo, X.; Xu, F.; Li, Y. F.; Hou, J. H. *Angew. Chem., Int. Ed.* **2011**, *50*, 9697.
(43) Zhang, M.; Gu, Y.; Guo, X.; Liu, F.; Zhang, S.; Huo, L.; Russell, T. P.; Hou, J. H. *Adv. Mater.* **2013**, DOI: 10.1002/adma.201301494.
(44) Voroshazi, E.; Vasseur, K.; Aernouts, T.; Heremans, P.; Baumann, A.; Deibel, C.; Xue, X.; Herring, A. J.; Lada, T. A.; Richter, H.; Rand, B. P. *J. Mater. Chem.* **2011**, *21*, 17345.
(45) Melzer, C.; Koop, E. J.; Mihailetchi, V. D.; Blom, P. W. *Adv. Funct. Mater.* **2004**, *14*, 865.
(46) Zhou, E.; Wei, Q.; Yamakawa, S.; Zhang, Y.; Tajima, K.; Yang, C.; Hashimoto, K. *Macromolecules* **2010**, *43*, 821.
(47) Pommerehne, J.; Vestweber, H.; Guss, W.; Mahrt, R. F.; Bassler, H.; Porsch, M.; Daub, J. *Adv. Mater.* **1995**, *7*, 551.
(48) Liang, Y.; Feng, D.; Wu, Y.; Tsai, S. T.; Li, G.; Ray, C.; Yu, L. P. *J. Am. Chem. Soc.* **2009**, *131*, 7792.
(49) Bredas, J. L.; Beljonne, D.; Coropceanu, V.; Cornil, J. *Chem. Rev.* **2004**, *104*, 4971.
(50) Thompson, B. C.; Fréchet, J. M. *Angew. Chem., Int. Ed.* **2008**, *47*, 58.
(51) Scharber, M. C.; Muhlbacher, D.; Koppe, M.; Denk, P.; Waldauf, C.; Heeger, A. J.; Brabec, C. J. *Adv. Mater.* **2006**, *18*, 789.
(52) Wu, P. T.; Kim, F. S.; Champion, R. D.; Jenekhe, S. A. *Macromolecules* **2008**, *41*, 7021.
(53) Huo, L.; Ye, L.; Wu, Y.; Li, Z.; Guo, X.; Zhang, M.; Zhang, S.; Hou, J. *Macromolecules* **2012**, *45*, 6923.
(54) Raghunath, P.; Reddy, M. A.; Gouri, C.; Bhanuprakash, K.; Rao, V. J. *J. Phys. Chem. A* **2006**, *110*, 1152.
(55) Holcombe, T. W.; Norton, J. E.; Rivnay, J.; Woo, C. H.; Goris, L.; Piliego, C.; Griffini, G.; Sellinger, A.; Brédas, J. L.; Salleo, A.; Fréchet, J. M. J. *J. Am. Chem. Soc.* **2011**, *133*, 12106.
(56) Brabec, C. J.; Cravino, A.; Meissner, D.; Sariciftci, N. S.; Fromherz, T.; Rispens, M. T.; Sanchez, L.; Hummelen, J. C. *Adv. Funct. Mater.* **2001**, *11*, 374.

NOTE ADDED AFTER ASAP PUBLICATION

This article posted ASAP on December 12, 2013. Column headings 2 and 3 in Table 1 have been revised. The correct version posted on December 16, 2013.